Precursory Migration of Anomalous Seismic Activity Revealed by the Pattern Informatics Method: A Case Study of the 2011 Tohoku Earthquake, Japan

by Masashi Kawamura, Yi-Hsuan Wu, Takeshi Kudo, and Chien-chih Chen

Abstract Anomalous seismicity patterns in epicentral and surrounding areas have been shown to occur prior to large earthquakes, although the processes determining the spatial distribution and migration patterns of such seismicity are still poorly understood. We applied the improved pattern informatics (PI) method to earthquake data maintained by the Japan Meteorological Agency (JMA) for a broad region including northeastern inland Japan and the source area of the 2011 Tohoku earthquake, in order to reveal the precursory processes of the earthquake and its related statistical features. In particular, we focused on the spatial distribution and migration patterns of PI hotspots, which highlight areas of anomalous seismic activity. Our results show that such hotspots had been approaching the epicenter of the 2011 Tohoku earthquake from 2000 until the earthquake occurred. The possibility that this result was obtained by chance was rejected at the 95% confidence level based on Molchan's error diagram. Our result supports the hypothesis that the preparatory processes of the 2011 Tohoku earthquake included anomalous seismic activity and its migration toward the epicenter of the earthquake.

Introduction

The 2011 Tohoku earthquake, with a moment magnitude (M_w) of 9.0, occurred off the Pacific coast of northeastern Japan on 11 March 2011; it was a thrust earthquake that occurred at a depth of about 24 km at the plate boundary where the Pacific plate subducts westward beneath the Okhotsk plate (Apel *et al.*, 2006). The occurrence of such a large earthquake was not anticipated because no earthquake with $M_w > 8.5$ has been reported along the Japan trench since the seventeenth century. However, temporal changes in seismic activity near the epicenter of the Tohoku earthquake were reported one month before its occurrence (Hirose *et al.*, 2011). Furthermore, the strain accumulation rate estimated from recent geodetic observations is much higher than that expected from the average strain released by previous interplate earthquakes (Nishimura *et al.*, 2004; Suwa *et al.*, 2006; Hashimoto *et al.*, 2009). This evidence implies that an enormous amount of stress had accumulated gradually in the locked area over a long time (Toya and Kasahara, 2005).

Seismic activity is a representative measure of tectonic stress acting on local regions. Therefore, it is prudent to focus on temporal change in seismic activity as a stress sensor. Anomalous seismic activity, for example, seismic activation and quiescence prior to the occurrence of large earthquakes, has been reported in seismically active regions worldwide (Resenberg and Matthews, 1988; Sykes and Jaume, 1990; Wyss and Wiemer, 1997; Jaume and Sykes, 1999; Bowman and King, 2001; Chen, 2003; Chen *et al.*, 2005; Chen and Wu, 2006; Wu and Chiao, 2006; Wu and Chen, 2007; Wu *et al.*, 2008a; Papazachos *et al.*, 2010; Mignan, 2011). With regard to large earthquakes in northeastern Japan, the occurrence of precursory seismic quiescence prior to the 1983 Nihonkai-Chubu earthquake, the 1989 off-Sanriku earthquake, the 2003 northern Miyagi earthquake, the 2003 Tokachi-oki earthquake, and the 2011 Tohoku earthquake has been reported by Murru *et al.* (1999), Wyss *et al.* (1999), Ogata (2005), Katsumata (2011a,b), respectively. Furthermore, the migration of anomalous seismic activity has also been reported in northeastern Japan, although its mechanism remains to be resolved (Mogi, 1968, 1969, 1973; Anderson, 1975; Kasahara, 1979).

These reports imply that there exists anomalous seismicity change associated with large earthquakes, occurring at their epicenters and in surrounding regions over periods a few years to decades before the occurrence of the earthquakes themselves. Examination of the precursory seismic activity of the 2011 Tohoku earthquake would provide important insight into the preparatory processes and anomalous seismic activity prior to such earthquakes. With this motivation, we investigated precursory seismicity changes associated with the Tohoku earthquake using the improved pattern
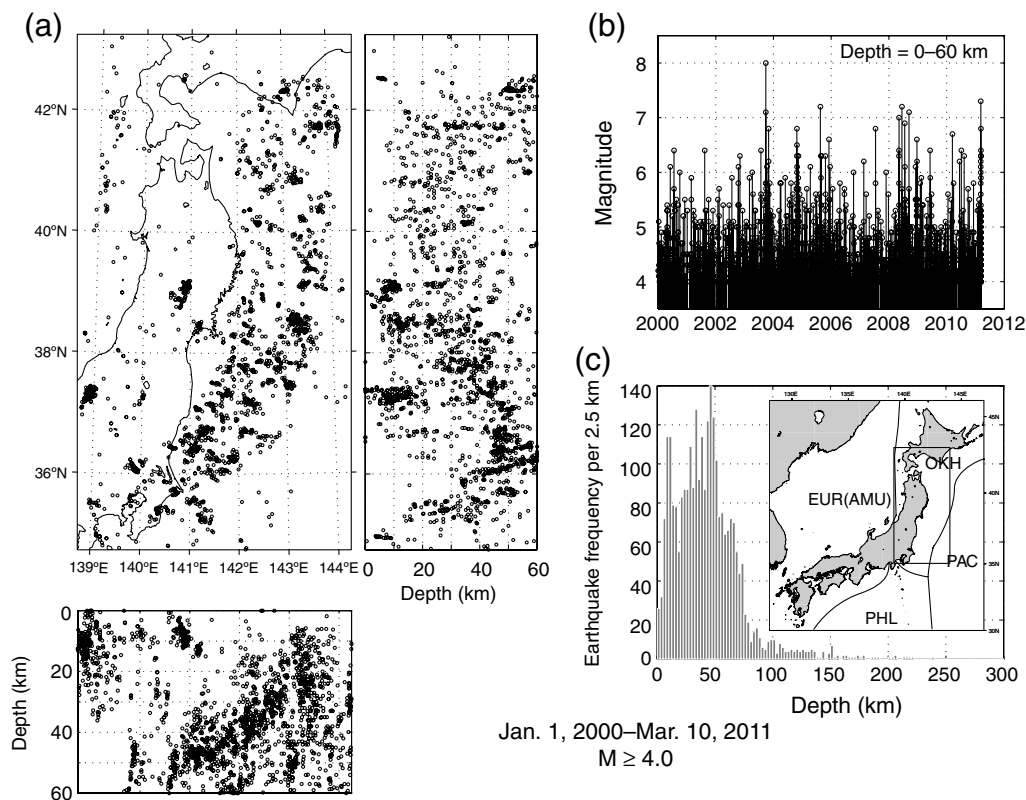
Figure 1.   (a) Hypocenter distribution at depths shallower than 60 km during 1 January 2000–10 March 2011. (b) Plots of magnitude versus time obtained using the events at depths of 0–60 km. (c) Histogram of earthquake frequency (**M** ≥ 4.0) versus the depth of its occurrence. Each bar denotes earthquake frequency within a depth window of 2.5 km at different depths. The inset shows a map view of the tectonic setting around the Japanese islands; PAC, Pacific plate; PHL, Philippine Sea plate; EUR (AMR), Eurasian plate (Amurian plate); OKH, Okhotsk plate. Black rectangle denotes the region for analysis in this study.

informatics (PI) method (Wu *et al.*, 2011) together with the original PI method, which has retrospectively identified anomalous seismic activities prior to large earthquakes (Chen *et al.*, 2005, 2006; Wu *et al.*, 2008b, 2011). In particular, we focused on the migration pattern of areas exhibiting anomalous seismicity changes (PI hotspots) by applying the improved PI method (Wu *et al.*, 2011), in which the error distance is defined as the distance between each grid cell in a target region for analysis and the nearest PI hotspot. Use of the concept of error distance (Wu *et al.*, 2011) has the advantage of displaying the approach of PI hotspots toward the epicenter of a future large earthquake. In other words, the decrease of error distance with time is related to the stress accumulation process around the epicenter of a future large earthquake. Therefore, study of error distance has the capacity to illuminate the preparatory process for a large earthquake. In the Data and Methodology section, we introduce the original PI method and the improved PI method incorporating the error distance. We further define the concept of integrated error distance to remove the dependence of an area of anomalous seismicity, or the number of grid cells defined as a PI hotspot, on threshold settings. We produce a PI map showing the spatial distribution of PI hotspots and a PI migration pattern map that illustrates the spatial distribu-

tion of the slope obtained by applying a linear regression to plots of integrated error distance against time before the Tohoku earthquake. The comparison of the migration pattern with the slip-deficit rate distribution on the plate boundary (Nishimura *et al.*, 2004; Suwa *et al.*, 2006) and the *P*-wave velocity distribution above the upper boundary of the subducting Pacific plate (Zhao *et al.*, 2011) shows that the region toward which anomalous seismicity areas migrate coincides with a zone of high slip-deficit rate and high velocity. We believe that this supports the hypothesis that PI migration is related to the preparatory process (stress accumulation process) of the 2011 Tohoku earthquake.

Data and Methodology

We used the earthquake catalog maintained by the Japan Meteorological Agency (JMA) (Fig. 1). In order to perform efficient data processing, the JMA unified earthquake catalogs maintained by different organizations, such as universities and research institutes, in October 1997. Furthermore, it started relocating past events using different velocity models and started changing the method for calculating magnitude (JMA magnitude) in 2003. Variation in seismic networks and data processing methods inevitably caused inhomogeneity in the earthquake catalog (Habermann, 1987; Resenberg

and Matthews, 1988). Thus, the spatial and temporal homogeneity of the JMA earthquake catalog is indispensable for evaluating temporal changes in seismic activity. In order to examine the homogeneity of the JMA earthquake catalog, we divided the region for analysis (Fig. 1) into grid cells of 0.25° by 0.25° and mapped minimum magnitude of completeness (M_c) for depth ranges of 0–100 km (shallower and deeper parts) and 60–100 km (only deeper parts) for each year since 2000 using the method of Wiemer and Wyss (2000). In order to calculate M_c for each grid cell, its surrounding 200 earthquakes were used. Application of this method obtained $M_c < 4.0$ for both depth ranges. Therefore, we here used events with JMA magnitude equal to or larger than 4.0 ($M \geq 4.0$) to calculate the change in seismic activity for each change interval. For simplicity, JMA magnitude is hereinafter represented as **M**.

Here, we have based determination of the depth range of events used for analysis on a statistical measure for evaluating ergodicity of an earthquake fault system: the Thirumalai-Mountain (TM) metric (Tiampo *et al.*, 2007, 2010; Toya *et al.*, 2010). If the earthquake fault system is ergodic, the inverse of the TM metric increases linearly with time, which means that the temporal average of a quantity approaches its ensemble average. Improvements in catalog quality can also cause a break in ergodicity of the system. We examined ergodicity of events at depths of 0–30 km, 0–60 km, and 0–100 km (Fig. 2). The plots of the inverse TM metric in panels (a) and (b) (0–30 km and 0–60 km, respectively) display clear linearity. Considering that the hypocenter of the 2011 Tohoku earthquake was located at a depth of 24 km and the lower limit of earthquake distribution in inland Japan is nearly 30 km (Fig. 1), the selection of events within 0–30 km appears to be sufficient for PI analysis. However, Ogata and Umino (2009) attempted to relocate the hypocenters of earthquakes in a region far offshore of northeastern Japan, and showed that most $M \geq 3.0$ events at depths of 40 km or more from 2000 until 2006 were relocated to depths shallower than 40 km. This indicates that the location errors of offshore events, most of which are shallower than 60 km, are large due to poor coverage of the seismic network in ocean regions. Furthermore, a depth of 60 km nearly corresponds to the bottom of the seismogenic zone associated with thrust events at the plate interface between the subducting Pacific plate and the overriding North American plate in this region. This depth is almost the same at other subduction zones (Corbi *et al.*, 2011; Heuret *et al.*, 2011). In addition, a simulation result by Kato *et al.* (1997) suggests that the seismic activity at the interface between subducting and overriding plates and in the continental crust can be affected by aseismic sliding at deeper parts of locked zones at the plate interface. These previous studies imply that it is more desirable to use events at depths of 0–60 km than those shallower than 30 km; thus, we opted to include all events shallower than 60 km in our study, which should make it possible to focus on changes in seismic activity in the continental crust and around the plate interface.
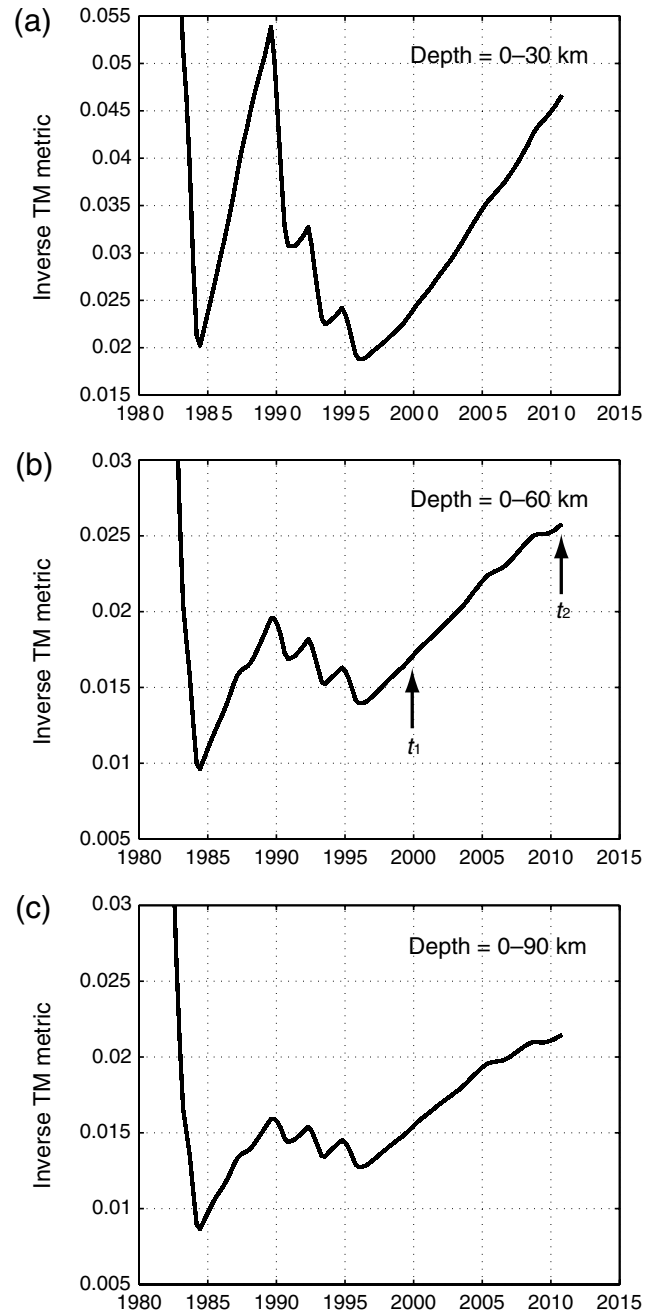
Figure 2. Plots of the inverse of the TM metric as a function of time using events at depths of (a) 0–30 km, (b) 0–60 km, and (c) 0–90 km. Black arrows, the beginning of t_1 and t_2.

The PI method was developed based on the concept of pattern dynamics (Rundle *et al.*, 2000). Stress, which can be regarded as a space–time state variable in a system of true deterministic dynamics, is a fundamental measure that should be monitored to help predict the occurrence of future large earthquakes, but it is difficult to observe directly. We can, however, observe seismic activity, which is considered to reflect stress rate (Dieterich, 1994; Dieterich *et al.*, 2000; Toda *et al.*, 2002). Therefore, in studying the preparatory

(a)

$\bar{I}$: Temporal mean of I

$\langle I \rangle$: Spatial mean of I

σ_I : Standard deviation of I

Start of making PI map for each change interval $t1$–$t2$ ($t2$ fixed)

Defining the following fixed parameters:
• Beginning time of earthquakes used for analysis: $t0$ (fixed)
• Time grid interval: Δt
• Ending time of change interval and of earthquakes used for analysis: $t2$ (fixed)
• Bounds of analysis region (e.g. longitudes and latitudes): $xlong\_min, xlong\_max, xlat\_min, xlat\_max$
• Spatial grid interval: Δx

Hypocenter catalog

Setting beginning time of change interval: $t1$
($t1 = t1start, t1start+\Delta t, t1start+2\Delta t,..., t1end$)

Setting sampling reference time: tb
($tb = t0, t0+\Delta t, t0+2\Delta t,..., tb end(< t1)$)

Setting calculation grid cell: xi ($i = 1$–n)

Calculating seismic intensity for the time interval of tb–$t1$ and tb–$t2$ in grid cell xi:
$$I_i(t_b,t_1) = \frac{1}{t_1 - t_b}\int_{t_b}^{t_1} n_i(t)dt \quad \text{and} \quad I_i(t_b,t_2) = \frac{1}{t_2 - t_b}\int_{t_b}^{t_2} n_i(t)dt$$
$n_i(t)$: Number of events occurring in grid cell xi and its specified neighbors

Calculating seismic intensity change for $t1$–$t2$ in grid cell xi:
$$\Delta I_i(t_b,t_1,t_2) = I_i(t_b,t_2) - I_i(t_b,t_1)$$

$x_{i+1} = x_i + \Delta x$ No   — $x_i = x_n$?   Yes

$t_b = t_b + \Delta t$ No   — $t_b = t_1$?   Yes

$t_1 = t_1 + \Delta t$

Calculating temporal normalization of seismic intensity change (as to tb):
$$\Delta \bar{I}_i(t_b,t_1,t_2) = \frac{\Delta I_i(t_b,t_1,t_2) - \overline{\Delta I_i(t_b,t_1,t_2)}}{\sigma_{\Delta I_i}}$$

Calculating spatial normalization of temporally normalized seismic intensity change:
$$\Delta \hat{I}_i(t_b,t_1,t_2) = \frac{\Delta \bar{I}_i(t_b,t_1,t_2) - \langle \Delta \bar{I}_i(t_b,t_1,t_2) \rangle}{\sigma_{\Delta \bar{I}_i}}$$

Calculating earthquake occurrence probability (Temporal mean square (as to tb) of spatio-temporally normalized seismic intensity change):
$$P_i(t_1,t_2) \equiv \overline{\left| \Delta \hat{I}_i(t_b,t_1,t_2) \right|^2}$$

Calculating earthquake occurrence probability relative to averaged background probability (subtracting spatial mean of Pi from Pi):
$$\Delta P_i(t_1,t_2) = P_i(t_1,t_2) - \langle P_i(t_1,t_2) \rangle$$

$$PI\ value \equiv \Delta P_i(t_1,t_2) / \max_i(\Delta P_i(t_1,t_2))$$
is color coded and plotted on the map.

$t_1 = t_{1end}$?   No / Yes

End

(b)   PI map (for each change interval $t1$–$t2$)

PI hotspot (grid cell with *PI value* higher than a threshold, or with high earthquake occurrence probability after $t2$)

Distance between grid cell xi and its nearest hotspot: Error distance ε

Calculation grid box xi

Plots of ε_area vs. change interval $t1$–$t2$ (for each calculation grid cell xi)

ε_area

$t1$

Area of PI hotspots (A_H) relative to area of analysis region (A): A_H/A

ε

Integration

Integrated error distance (for each grid cell xi and change interval $t1$–$t2$: ε_area

ε_area

$0 \quad A_H/A \quad 1$

PI migration map

Color coded and plotted on the map
ex. Slope negative: blue
positive: red
zero: green

Figure 3. (a) Flowchart of the procedure for obtaining PI maps, which denote the spatial distribution of grid cells with earthquake occurrence probabilities higher than a particular threshold (PI hotspots). (b) Schematic diagram of the method for obtaining a PI migration map based on PI maps obtained by the process illustrated in (a).

process of a large earthquake, we regarded seismic activity as a space–time state variable of pattern dynamics that can be incorporated into investigation of changes in an earthquake system.

We applied the PI method to earthquake data covering a broad region that included northeastern inland Japan and the epicenter of the 2011 Tohoku earthquake, in order to obtain a precursory earthquake-migration pattern. Figure 3a illustrates the procedure for obtaining PI maps, which denote the spatial distribution of grid cells with earthquake occurrence probabilities higher than a particular threshold (PI hotspots). Figure 3b illustrates the method for obtaining a PI migration

map based on PI maps obtained by the process illustrated in Figure 3a. The PI migration map shows whether or not the nearest PI hotspot is, on average, approaching the grid cell with time, viewed from each grid cell. We here explain the PI analysis procedure.

1. The target region is divided into grid cells with dimensions of $0.25° \times 0.25°$.
2. Seismic-intensity change $\Delta I_i(t_b, t_1, t_2)$ of the ith grid for a target time period (change interval), that is, from t_1 to t_2 ($t_1 = 1$ January 2000–1 January 2008, $t_2 = 1$ January 2011), is calculated. The seismic intensity $I_i(t_b, t)$ is defined as the number of earthquakes per day in an area of 5×5 grids, centered at the ith grid cell, averaged over the time period between a reference time $t_b(t_0 < t_b < t_1)$ and t. To obtain the seismic-intensity change, the seismic intensities $I_i(t_b, t_1)$ and $I_i(t_b, t_2)$ in the ith grid cell for the respective time period, that is, t_b to t_1 and t_b to t_2, are calculated. Then, we calculate seismic-intensity change $\Delta I_i(t_b, t_1, t_2) = I_i(t_b, t_2) - I_i(t_b, t_1)$. In this study, the beginning of t_1 is selected based on the property of ergodicity of a natural earthquake fault system, which can be identified using the inverse of the TM metric (Fig. 2b). The inverse TM metric on 1 January 2000 nearly corresponds to the beginning of the linearity evident in Figure 2b. Thus, we select 1 January 2000 as the beginning of t_1.
3. To extract the coherent trends in seismic-intensity change during t_1 to t_2, the seismic intensities $I_i(t_b, t_1)$ and $I_i(t_b, t_2)$ are calculated by shifting t_b from t_0 (1 January 1980) to t_1; thus, the seismic-intensity change $\Delta I_i(t_b, t_1, t_2)$ can be normalized temporally by subtracting its temporal mean and dividing by its temporal standard deviation. Furthermore, $\Delta I_i(t_b, t_1, t_2)$ is also normalized spatially to highlight unusual seismic-intensity changes. The value of $\Delta I_i(t_b, t_1, t_2)$ varies according to the grid cells where t_b is fixed; therefore, we can normalize it spatially by subtracting its spatial mean and then dividing by its spatial standard deviation for every value of t_b. The spatiotemporally normalized seismic-intensity change is then obtained and denoted as $\Delta \hat{I}_i(t_b, t_1, t_2)$.
4. Most of the effects of random fluctuation in seismic-intensity change and background seismic-intensity change are eliminated by normalization. Accordingly, the preseismic change can be represented by the spatiotemporally normalized seismic-intensity change $\Delta \hat{I}_i(t_b, t_1, t_2)$. Because the preseismic change during a preparatory process can be seismic quiescence, seismic activation, or even both, $\Delta \hat{I}_i(t_b, t_1, t_2)$ may be negative or positive. To incorporate all the preseismic change and reduce the fluctuation of random noise, we take the absolute value of spatiotemporally normalized seismic intensity $|\Delta \hat{I}_i(t_b, t_1, t_2)|$ and average the absolute value over all values of t_b to obtain $\overline{|\Delta \hat{I}_i(t_b, t_1, t_2)|}$.
5. Then, the probability of earthquake occurrence $P_i(t_1, t_2)$ is defined as $\overline{|\Delta \hat{I}_i(t_b, t_1, t_2)|}^2$ and the average probability as the mean μ_p of $P_i(t_1, t_2)$. Finally, the probability of

earthquake occurrence relative to the background mean, $\Delta P_i(t_1, t_2) \equiv \overline{|\Delta \hat{I}_i(t_b, t_1, t_2)|}^2 - \mu_p$, is further divided by the spatial maximum and is color coded and plotted as a PI hotspot.

6. In order to draw a PI migration map, the error distance ε is defined as the distance between each grid cell and its nearest hotspot. Thus, the error distance is defined for each grid cell for each change interval from t_1 to t_2. It should, however, be noted that the total area of PI hotspots depends on the threshold value of the probability of earthquake occurrence; the higher the threshold value, the less the total area of PI hotspots. Accordingly, the error distance would decrease (increase) with increasing (decreasing) ratio of the area of PI hotspots (A_H) to the area of the whole region used for analysis (A). In order to eliminate the influence of threshold settings of PI hotspots on the result, we instead consider the integrated error distance, $\varepsilon_{\mathrm{area}}(t_1)$, which is obtained by integrating the plots of ε as a function of A_H/A, in studying the temporal change in the distance between each grid cell and its nearest PI hotspot.
7. By shifting t_1, the temporal change in the integrated error distance defined in step 6 is obtained for every grid cell. To make it possible for the migration of PI hotspots to be observed in time and space, we apply a linear regression to the plotted integrated error distance as a function of time (t_1) for each grid cell and color code on the map.

Results

Figure 4 shows snapshots of the spatial distribution of the grid cells with large seismicity changes (PI hotspots) for different change intervals between t_1 and t_2 ($t_2 = 1$ January 2011), or snapshots of PI maps. Warm colors indicate the locations with large seismicity changes over the change interval, including seismic quiescence and activation, indicating high probability of earthquake occurrence after the change interval; red corresponds to the highest probability of earthquake occurrence. Cold colors represent the locations with small seismicity changes, indicating low probability of earthquake occurrence after the change interval. It should be noted that the blue areas include all occurrence probabilities lower than -0.6. The red star in each panel shows the epicenter of the 2011 Tohoku earthquake. It can be seen that PI hotspots, or the grid cells with anomalous seismicity, approach the epicenter of the 2011 Tohoku earthquake. Furthermore, we have calculated the integrated error distance as a function of time for every grid cell and plotted the migration pattern of PI hotspots (Fig. 5) to investigate the overall migration of the grid cells with anomalous seismicity changes during the period shown in the top of Figure 5a. If the distance decreases with time (negative slope), the corresponding grid cells are light blue to blue in color. On the contrary, if the distance increases with time (positive slope), the corresponding grids are colored yellow to red. The migration patterns shown in Figure 5a were obtained using $t_1 = 1$ January 2000–1 January 2008.
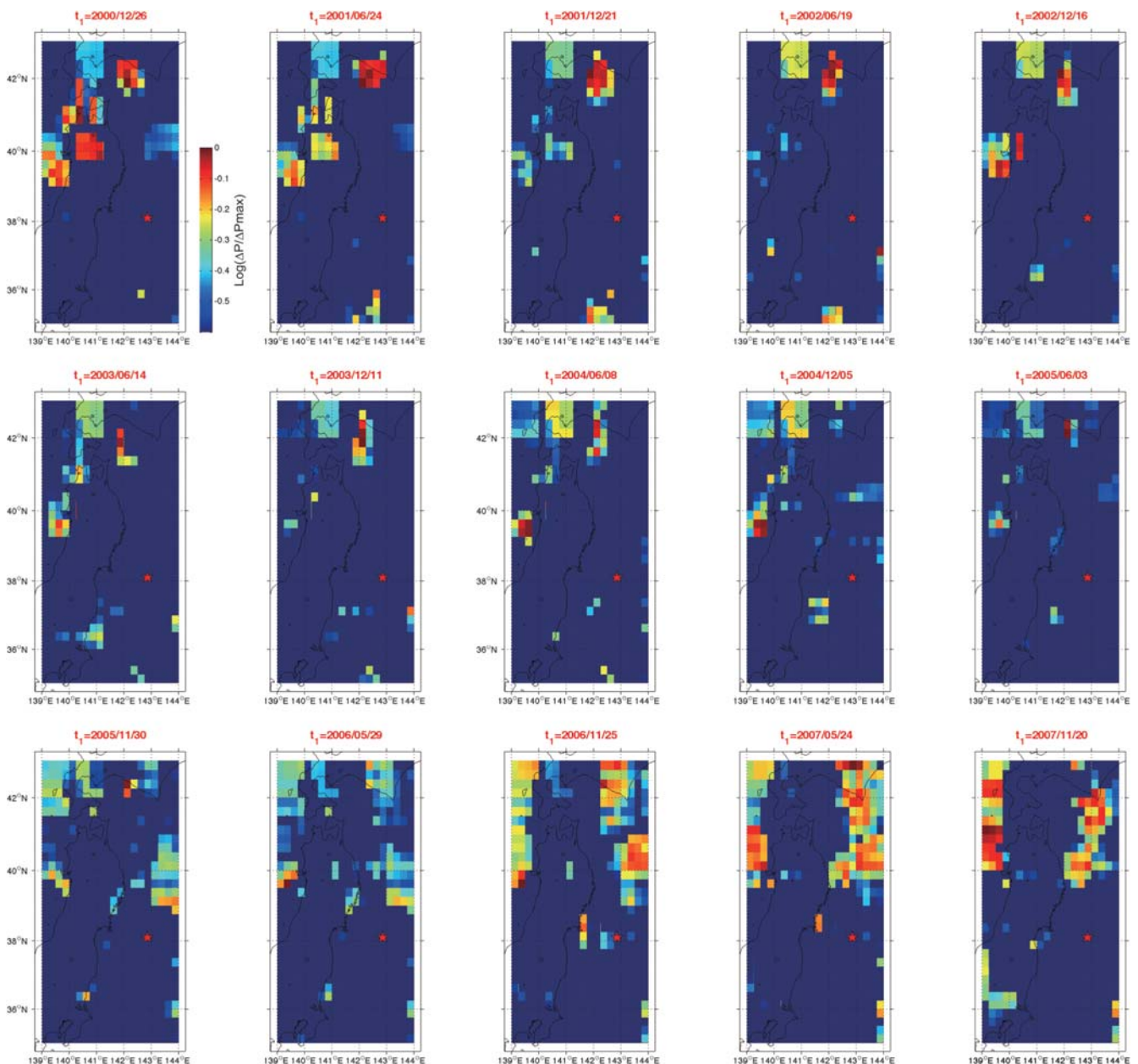
Figure 4. Snapshots of the spatial distribution of the grid cells with large seismicity changes (PI hotspots) for different change intervals between t_1 and t_2 ($t_2 = 1$ January 2011). Change interval for each panel is shown at top (only t_1 is denoted). Warm-color grid cells show the locations with large seismicity changes, including seismic quiescence and activation, during the change interval; this indicates high probability of earthquake occurrence after the change interval. Red-color regions correspond to the highest probability of earthquake occurrence. Cold colors represent locations with small seismicity changes, indicating low probability of earthquake occurrence after the change interval. It should be noted that the blue regions include all occurrence probabilities lower than −0.6. It can be seen that the locations of the PI hotspots, which are regarded as anomalous seismicity areas, approach the epicenter of the 2011 Tohoku earthquake, which is indicated by the red star.

The **M** ≥ 5.0 events during the time period from t_2 (1 January 2011) to 10 March 2011, one day before the occurrence of the Tohoku earthquake are also plotted (black open circles). A large region of negative slope is evident between 38° N and 39° N in the PI migration pattern (Fig. 5a), suggesting that this region has high potential for earthquake occurrence; this region includes the epicenter of the Tohoku earthquake. Figure 5b shows plots of the integrated error distance as a function of change interval for two grid cells indicated by

arrows; one of the grid cells includes the epicenter of the 2011 Tohoku earthquake. The horizontal axis denotes t_1, which represents the change interval between t_1 and t_2; the vertical axis shows the integrated error distance for each corresponding change interval. The negative slope obtained by fitting a linear regression to these plots reflects the relative movement of PI hotspots toward the epicenter of the 2011 Tohoku earthquake with time. Figure 5b also implies that PI hotspots migrate by nearly 200–300 km, on average, toward
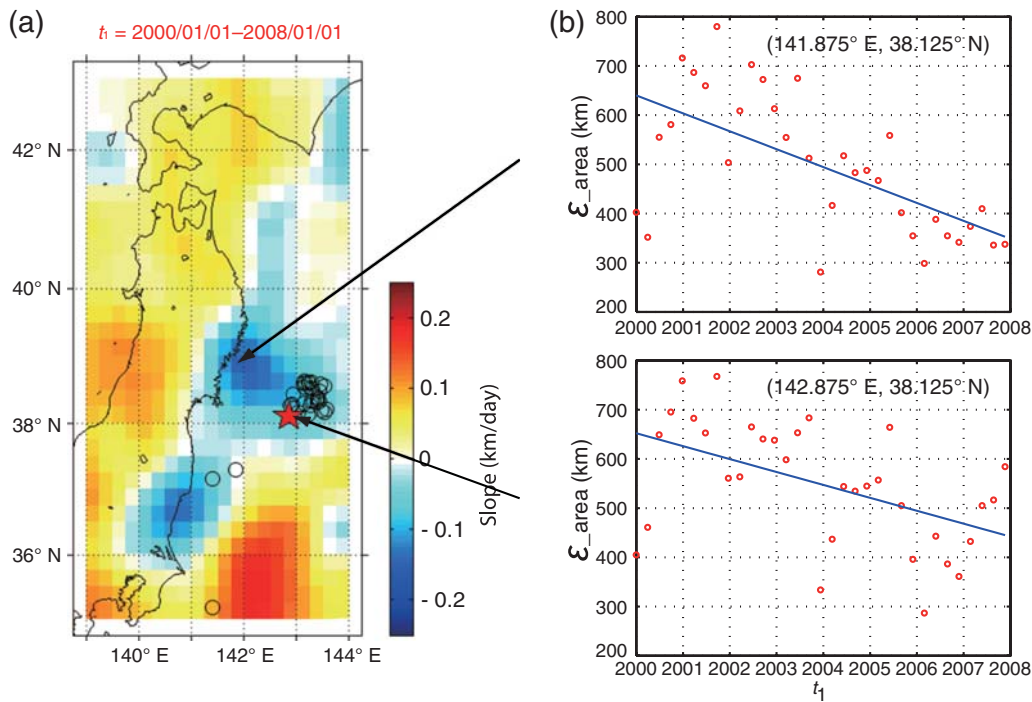
Figure 5. (a) PI migration pattern map: map showing the temporal change in the integrated error distance between each grid cell and its nearest PI hotspot. The map shown was obtained by using $t_1 = $ 1 January 2000–1 January 2008. Red star denotes the epicenter of the 2011 Tohoku earthquake. Black open circles show the epicenters of $\mathbf{M} \geq 5.0$ earthquakes shallower than 60 km for the period between t_2 (1 January 2011) and 10 March 2011, one day before the occurrence of the Tohoku earthquake. If the integrated error distance decreases with time, the corresponding grid cells are shown with light blue to blue color. On the contrary, if the integrated error distance increases with time, the corresponding grid cells are denoted with yellow to red color. (b) Plots of integrated error distance as a function of change interval for two grid cells, (141.875° E, 38.875° N) and (142.875° E, 38.125° N). Horizontal axis denotes t_1, which is substituted for change interval between t_1 and t_2. Negative slopes (blue lines) obtained by linear regression fitting to the plots reflect the approach of PI hotspots to the two grid cells with time; one of these includes the epicenter of the 2011 Tohoku earthquake.

the patch bounded by the lines at 38° N and 39° N and including the epicenter of the 2011 Tohoku earthquake for the period from 1 January 2000 to 1 January 2008. Therefore, Figures 4 and 5 indicate that the PI hotspots migrate toward the epicenter over time.

To evaluate the coherence between the epicenter of the Tohoku earthquake and the regions of negative slope in the PI migration map, we used Molchan's error diagram (Fig. 6; Molchan, 1997). Figure 6 plots miss rate versus the fraction of grid cells with negative slopes, which indicate the approach of PI hotspots toward the grid cells. Here, miss rate is defined as the number of $\mathbf{M} \geq 5.0$ events located outside the grid cells with negative slopes, normalized by the total number of $\mathbf{M} \geq 5.0$ events. In calculating the lower 95% confidence level of the random miss rate, we used the method of Zechar and Jordan (2008). The best performance of the improved PI method is denoted by a black arrow in Figure 6. Based on the actual miss rate and fraction of grid cells with negative slopes, denoted as a large solid circle in Figure 6, the null hypothesis that the coherence between the locations of $\mathbf{M} \geq 5.0$ events and the grid cells with negative slopes is obtained by chance is rejected at a confidence level of 95%. This indicates good performance of the improved PI method

in identifying $\mathbf{M} \geq 5.0$ events, including the 2011 Tohoku earthquake, inside grid cells with negative slopes.

Discussion and Conclusions

We applied the PI method to the earthquake catalog of the region east of northeastern Japan prior to the occurrence of the 2011 Tohoku earthquake. Seismicity rate is a proxy for stress rate (Dieterich, 1994; Dieterich *et al.*, 2000; Toda *et al.*, 2002). Therefore, the positions of PI hotspots indicate areas with significant temporal changes in stress rates over change interval. In this study, we focused on the migration pattern of PI hotspots. Where PI hotspots approach the epicenter of large earthquakes, the stress rate around the hypocenter area increases with time. Thus, it is physically reasonable to assume that the direction of migration of PI hotspots can help predict the epicenter of future large earthquakes. Figures 4 and 5 show that PI hotspots approached the epicenter of the 2011 Tohoku earthquake prior to its occurrence. This may reflect stress accumulation toward the region near the epicenter. Interestingly, the blue region including the epicenter of the Tohoku earthquake in Figure 5a almost coincides with a strongly coupled region between the Pacific plate and the overriding North American plate (Nishimura *et al.*, 2004;
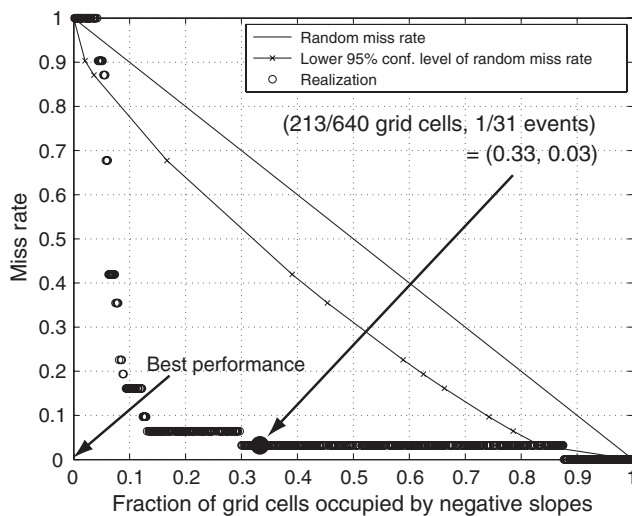
Figure 6. Molchan's error diagram which plots miss rate versus the fraction of grid cells occupied by negative slopes, showing the approach of PI hotspots to grid cells under consideration. Here, miss rate is defined as the number of $M \geq 5.0$ events located outside grid cells of negative slopes, normalized by the total number of $M \geq 5.0$ events. Plots show random miss rate (line connecting [0,1] to [1,0]), lower 95% confidence level of random miss rate (curve with black cross connecting [0,1] to [1,0]), and realizations obtained by changing the threshold of negative slopes (positive maximum slope to negative maximum slope) (black open circle). Best performance of the improved PI method occurs in the bottom left corner, and is denoted by a black arrow. The actual miss rate and fraction of grid cells occupied by negative slopes is denoted by a large solid circle.

Suwa *et al.*, 2006; Hashimoto *et al.*, 2009; Ozawa *et al.*, 2011). This region also corresponds to a region with coseismic slips larger than ~25 m (Iinuma *et al.*, 2011; Ozawa *et al.*, 2011), and with a region of high *P*-wave velocity directly above the upper boundary of the subducting Pacific plate (Huang *et al.*, 2011; Zhao *et al.*, 2011). These coincidences imply that the blue region corresponds to a large asperity on the plate boundary where stress tends to accumulate. Using the JMA earthquake catalog with $M \geq 4.5$ and depths shallower than 60 km, Katsumata (2011a) found a region of anomalous seismic quiescence in the deeper part of the asperity ruptured by the Tohoku earthquake by means of a *Z* test (Wiemer and Wyss, 1994). The region including the epicenter of the Tohoku earthquake in our study, toward which PI hotspots migrate, could reflect this seismic quiescence to some degree. Figure 5b shows that the mean of the distance between the epicenter of the Tohoku earthquake and the nearest PI hotspot decreases with time. This may be due to the process of stress accumulation toward the large asperity including the hypocenter of the 2011 Tohoku earthquake. In this study, the asperity represented as a high-velocity zone, which was obtained previously by Zhao *et al.* (2011), is probably represented by the region of negative slopes (blue color) that the PI hotspots approach.

We consider here a possible mechanism for occurrence of seismic quiescence prior to the Tohoku earthquake.

Ohnaka (1984) proposed a precursory stable slip model for the boundary between a subducting plate and its overriding plate to explain the seismic quiescence period prior to a large interplate earthquake, based on the earthquake catalog and sea-level data in the Kanto region, Japan. Using the PI method, Wu *et al.* (2008b, 2011) demonstrated that areas with anomalous seismic activity, denoted as PI hotspots, migrated toward the epicenter of the 1999 Chi-Chi earthquake, Taiwan, insisting that migration of such areas may reflect the nucleation process of the earthquake. Using a numerical simulation involving rate- and state-dependent friction laws (Ruina, 1983), Kato *et al.* (1997) demonstrated the appearance of regional seismic quiescence in the continental crust before a large interplate earthquake, suggesting that regional stress relaxation could be caused by preseismic sliding along the boundary between a subducting oceanic plate and its overriding continental plate. The blue region toward which PI hotspots migrate over time in our study (Fig. 5a) may thus reflect a temporal change in seismicity associated with physical processes, including regional stress relaxation, prior to the Tohoku earthquake.

We conclude that the earthquake migration pattern obtained in this study supports the hypothesis of the preparatory stress accumulation process for the Tohoku earthquake since 2000. In future work, it will be important to investigate further the migration pattern associated with other large earthquakes, including intraplate earthquakes, to study the possibility of the improved PI method being used to image a region in which stress has accumulated to a large degree.

Data and Resources

We used the unified earthquake catalog maintained by the Japan Meteorological Agency (JMA), in which each hypocenter is determined by analyzing in an integrated fashion the earthquake data of Hokkaido University, Hirosaki University, Tohoku University, the University of Tokyo, Nagoya University, Kyoto University, Kochi University, Kyushu University, Kagoshima University, National Research Institute for Earth Science and Disaster Prevention (NIED), National Institute of Advanced Industrial Science and Technology (AIST), Japan Agency for Marine-Earth Science and Technology (JAMSTEC), Tokyo Metropolitan Government, Yokohama City, Shizuoka Prefecture, Hot Springs Research Institute of Kanagawa Prefecture, and JMA. Data can be obtained from the Japan Meteorological Business Support Center.

Acknowledgments

References

Anderson, D. L. (1975). Accelerated plate tectonics, *Science* **187,** 1077–1079.

Apel, E. V., R. Bürgmann, G. Steblov, N. Vasilenko, R. King, and A. Prytkov (2006). Independent active microplate tectonics of northeast Asia from GPS velocities and block modeling, *Geophys. Res. Lett.* **33,** L11303, doi: 10.1029/2006GL026077.

Bowman, D. D., and G. C. P. King (2001). Accelerating seismicity and stress accumulation before large earthquakes, *Geophys. Res. Lett.* **28,** 4039–4042.

Chen, C. C. (2003). Accelerating seismicity of moderate-size earthquakes before the 1999 Chi-Chi, Taiwan, earthquake: Testing time-prediction of the self-organizing spinodal model of earthquakes, *Geophys. J. Int.* **155,** F1–F5.

Chen, C. C., and Y. X. Wu (2006). An improved region-time-length algorithm applied to the 1999 Chi-Chi, Taiwan earthquake, *Geophys. J. Int.* **166,** 1144–1147.

Chen, C. C., J. B. Rundle, J. R. Holliday, K. Z. Nanjo, D. L. Turcotte, S. C. Li, and K. F. Tiampo (2005). The 1999 Chi-Chi, Taiwan, earthquake as a typical example of seismic activation and quiescence, *Geophys. Res. Lett.* **32,** L22315, 4 pp., doi: 10.1029/2005GL023991.

Chen, C. C., J. B. Rundle, H. C. Li, J. R. Holliday, K. Z. Nanjo, D. L. Turcotte, and K. F. Tiampo (2006). From tornadoes to earthquakes: Forecast verification for binary events applied to the 1999 Chi-Chi, Taiwan, earthquake, *Terr. Atmos. Ocean. Sci.* **17,** 503–516.

Corbi, F., F. Funiciello, C. Faccenna, G. Ranalli, and A. Heuret (2011). Seismic variability of subduction thrust faults: Insights from laboratory models, *J. Geophys. Res.* **116,** B06304, 14 pp., doi: 10.1029/2010JB007993.

Dieterich, J. (1994). A constitutive law for rate of earthquake production and its application to earthquake clustering, *J. Geophys. Res.* **99,** no. B2, 2601, doi: 10.1029/93JB02581.

Dieterich, J., V. Cayol, and P. Okubo (2000). The use of earthquake rate changes as a stress meter at Kilauea volcano, *Nature* **408,** 457–460.

Habermann, R. E. (1987). Man-made changes of seismicity rates, *Bull. Seismol. Soc. Am.* **77,** 141–159.

Hashimoto, C., A. Noda, T. Sagiya, and M. Matsu'ura (2009). Interplate seismogenic zones along the Kuril–Japan trench from GPS data inversion, *Nature Geosci.* **2,** 141–144.

Heuret, A, S. Lallemand, F. Funiciello, C. Piromallo, and C. Faccenna (2011). Physical characteristics of subduction interface type seismogenic zones revisited, *G-cubed* **12,** 26 pp., Q01004, doi: 10.1029/2010GC003230.

Hirose, F., K. Miyaoka, N. Hashimoto, T. Yamazaki, and M. Nakamura (2011). Outline of the 2011 off the Pacific coast of Tohoku earthquake (M_w 9.0) seismicity: Foreshocks, mainshock, aftershocks, and induced activity, *Earth Planets Space* **63,** 513–518.

Huang, Z., D. Zhao, and L. Wang (2011). Seismic heterogeneity and anisotropy of the Honshu arc from the Japan Trench to the Japan Sea, *Geophys. J. Int.* **184,** no. 3, 1428–1444, doi: 10.1111/j.1365-246X.2011.04934.x.

Iinuma, T., M. Ohzono, Y. Ohta, and S. Miura (2011). Coseismic slip distribution of the 2011 off the Pacific coast of Tohoku Earthquake (M 9.0) estimated based on GPS data: Was the asperity in Miyagi-oki ruptured? *Earth Planets Space* **63,** 643–648.

Jaume, S. C., and L. R. Sykes (1999). Evolving towards a circular point: A review of accelerating seismic moment/energy release prior to large and great earthquakes, *Pure Appl. Geophys.* **155,** 279–306.

Kasahara, K. (1979). Migration of crustal deformation, *Tectonophysics* **52,** 329–341.

Kato, N., M. Ohtake, and T. Hirasawa (1997). Possible mechanism of precursory seismic quiescence: Regional stress relaxation due to pre-seismic sliding, *Pure Appl. Geophys.* **150,** 249–267.

Katsumata, K. (2011a). A long-term seismic quiescence started 23 years before the 2011 off the Pacific coast of Tohoku Earthquake ($M = 9.0$), *Earth Planets Space* **63,** 709–712.

Katsumata, K. (2011b). Precursory seismic quiescence before the $M_\mathrm{w} = 8.3$ Tokachi-oki, Japan, earthquake on 26 September 2003 revealed by a re-examined earthquake catalog, *J. Geophys. Res.* **116,** B10307, 16 pp., doi: 10.1029/2010JB007964.

Mignan, A. (2011). Retrospective on the accelerating seismic release (ASR) hypothesis: Controversy and new horizons, *Tectonophysics* **505,** 1–16.

Mogi, K. (1968). Migration of seismic activity, *Bull. Earthq. Res. Inst. Tokyo Univ.* **46,** 53–74.

Mogi, K. (1969). Some features of recent seismic activity in and near Japan (2), *Bull. Earthq. Res. Inst. Tokyo Univ.* **46,** 30–36.

Mogi, K. (1973). Relationship between shallow and deep seismicity in the western Pacific region, *Tectonophysics* **17,** 1–22.

Molchan, G. M. (1997). Earthquake prediction as a decision making problem, *Pure Appl. Geophys.* **149,** 233–247.

Murru, M., R. Console, and C. Montuori (1999). Seismic quiescence precursor to the 1983 Nihonkai-Chubu (M 7.7) earthquake, Japan, *Ann. Geofisc.* **42,** 871–882.

Nishimura, T., T. Hirasawa, S. Miyazaki, T. Sagiya, T. Tada, S. Miura, and K. Tanaka (2004). Temporal change of interplate coupling in northeastern Japan during 1995–2002 estimated from continuous GPS observations, *Geophys. J. Int.* **157,** 901–916.

Ogata, Y. (2005). Detection of anomalous seismicity as a stress change sensor, *J. Geophys. Res.* **110,** B05S06, 14 pp., doi: 10.1029/2004JB003245.

Ogata, Y., and N. Umino (2009). Correction of routinely determined hypocenter coordinates in far offshore region, in *The 6th International Workshop on Statistical Seismology*, Granlibakken Conference Center, Lake Tahoe, California.

Ohnaka, M. (1984). A sequence of seismic activity in the Kanto area precursory to the 1923 Kanto earthquake, *Pure Appl. Geophys.* **122,** 848–862.

Ozawa, S., T. Nishimura, H. Suito, T. Kobayashi, M. Tobita, and T. Imakiire (2011). Coseismic and postseismic slip of the 2011 magnitude-9 Tohoku-Oki earthquake, *Nature* **475,** 373–376, doi: 10.1038/nature10227.

Papazachos, B. C., G. F. Karakaisis, E. M. Scordilis, C. B. Papazachos, and D. G. Panagiotopoulos (2010). Present patterns of decelerating-accelerating seismic strain in South Japan, *J. Seismol.* **14,** doi: 10.1007/s10950-009-9165-z.

Resenberg, P. A., and M. V. Matthews (1988). Precursory seismic quiescence: A preliminary assessment of the hypothesis, *Pure Appl. Geophys.* **126,** 373–406.

Ruina, A. L. (1983). Slip instability and state variable friction laws, *J. Geophys. Res.* **88,** 10,359–10,370.

Rundle, J. B., W. Klein, K. Tiampo, and S. Gross (2000). Linear pattern dynamics in nonlinear threshold systems, *Phys. Rev. E* **61,** 2418–2431.

Suwa, Y., S. Miura, A. Hasegawa, T. Sato, and K. Tachibana (2006). Interplate coupling beneath NE Japan inferred from three-dimensional displacement field, *J. Geophys. Res.* **111,** B04402, doi: 10.1029/2004JB003203.

Sykes, L. R., and S. C. Jaume (1990). Seismic activity on neighboring faults as a long-term precursor to large earthquakes in the San Francisco Bay area, *Nature* **348,** 595–599.

Tiampo, K. F., W. Klein, H.-C. Li, Y. Toya, S. Z. L. Kohen-Kadosh, J. B. Rundle, and C.-C. Chen (2010). Ergodicity and earthquake catalogs: Forecast testing and resulting implications, *Pure Appl. Geophys.* **167,** 763–782.

Tiampo, K. F., J. B. Rundle, W. Klein, J. Holliday, J. S. Sa Martines, and C. D. Ferguson (2007). Ergodicity in natural earthquake fault networks, *Phys. Rev. E* **75,** 066107, doi: 10.1103/PhysRevE.75.066107.

Toda, S., R. S. Stein, and T. Sagiya (2002). Evidence from the A.D. 2000 Izu islands earthquake swarm that stressing rate governs seismicity, *Nature* **419,** 58–61.

Toya, Y., and M. Kasahara (2005). Robust and exploratory analysis of active mesoscale tectonic zones in Japan utilizing the nationwide GPS array, *Tectonophysics* **400,** 27–53.

Toya, Y., K. F. Tiampo, J. B. Rundle, C.-C. Chen, H.-C. Li, and W. Klein (2010). Pattern informatics approach to earthquake forecasting in 3D, *Concurrency Comput. Pract. Ex.* **22,** no. 12, 1569–1592, doi: 10.1002/cpe.1531.

Wiemer, S., and M. Wyss (1994). Seismic quiescence before the Landers ($M = 7.5$) and Big Bear ($M = 6.5$) 1992 earthquakes, *Bull. Seismol. Soc. Am.* **84,** 900–916.

Wiemer, S., and M. Wyss (2000). Minimum magnitude of completeness in earthquake catalogs: Examples from Alaska, the western United States, and Japan, *Bull. Seismol. Soc. Am.* **90,** 859–869.

Wu, Y. H., C. C. Chen, and J. B. Rundle (2008a). Precursory seismic activation of the Pintung (Taiwan) offshore doublet earthquakes on 26 December 2006: A pattern informatics analysis, *Terr. Atmos. Ocean. Sci.* **19,** 743–749.

Wu, Y. H., C. C. Chen, and J. B. Rundle (2008b). Detecting precursory earthquake migration patterns using the pattern informatics method, *Geophys. Res. Lett.* **35,** L19304, 5 pp., doi: 10.1029/2008GL035215.

Wu, Y. H., C. C. Chen, and J. B. Rundle (2011). Precursory small earthquake migration patterns, *Terra Nova* **23,** 369–374.

Wu, Y. M., and C. C. Chen (2007). Seismic reversal pattern for the 1999 Chi-Chi, Taiwan, M_w 7.6 earthquake, *Tectonophysics* **429,** 125–132.

Wu, Y. M., and L. Y. Chiao (2006). Seismic quiescence before the 1999 Chi-Chi, Taiwan, M_w 7.6 earthquake, *Bull. Seismol. Soc. Am.* **96,** 321–327.

Wyss, M., and S. Wiemer (1997). Two current seismic quiescences within 40 km of Tokyo, *Geophys. J. Int.* **128,** 459–473.

Wyss, M., A. Hasegawa, S. Wiemer, and N. Umino (1999). Quantitative mapping of precursory seismic quiescence before the 1989, M 7.1 off-Sanriku earthquake, Japan, *Ann. Geofisc.* **42,** 851–869.

Zechar, J. D., and T. H. Jordan (2008). Testing alarm-based earthquake prediction, *Geophys. J. Int.* **172,** 715–724.

Zhao, D., Z. Huang, N. Umino, A. Hasegawa, and H. Kanamori (2011). Structural heterogeneity in the megathrust zone and mechanism of the 2011 Tohoku-oki earthquake, *Geophys. Res. Lett.* **38,** L17308, 5 pp., doi: 10.1029/2011GL048408.

Department of Earth Sciences and Graduate Institute of Geophysics
National Central University
Jhongli, Taoyuan 32001
Taiwan
mkawamu@ncu.edu.tw
    (M.K.)

Department of Geology
University of California
Davis, California 95616-8605
    (Y.-H.W.)

General Education Division, College of Engineering
Chubu University
Kasugai, Aichi 487-0027
Japan
    (T.K.)

Department of Earth Sciences and Graduate Institute of Geophysics
National Central University
Jhongli, Taoyuan 32001
Taiwan
    (C.C.)